Materials Advances

ROYAL SOCIETY OF CHEMISTRY

PAPER

View Article Online
View Journal | View Issue

Cite this: *Mater. Adv.*, 2025, **6**, 6001

Platinum catalyst-functionalized cylindrical graft copolymer micelles for dual catalytic and cytotoxic activity†

Kyosuke Seryu, Chieri Inada and Tomoki Nishimura *

Received 20th May 2025,
Accepted 15th July 2025

DOI: 10.1039/d5ma00518c

rsc.li/materials-advances

Catalytic prodrug activation offers a promising approach to cancer therapy, but integrating catalytic and therapeutic functions within a single platform remains challenging. In addition, low-molecular weight metal catalysts suffer from rapid clearance and limited *in vivo* efficacy. Here, we present a platinum complex-conjugated polymeric micellar system, constructed from amphiphilic poly(acrylic acid)-*graft*-poly(propylene oxide), which self-assembles into short cylindrical micelles (*ca.* 50 nm in length) in aqueous solution. The micelles are functionalized with a cisplatin-derived Pt(IV) metal complex, which is released under reductive conditions and converted into catalytically active Pt(II) species capable of deprotecting an *N*-propargylated 5-fluorouracil prodrug. The catalytic transformation proceeds more efficiently under mildly acidic conditions (pH = 6.0), achieving up to 35% conversion after 96 hours. Cell viability assays using CT26 cancer cells showed a decrease in viability from 60% (Pt-micelle alone) to below 50% when combined with the prodrug, indicating dual catalytic and cytotoxic activity *in vitro*. These findings provide a proof-of-concept for a dual-functional nanocarrier system capable of localized prodrug activation and therapeutic action, offering a promising strategy for advancing metal-catalyzed cancer therapy.

Introduction

Selective drug delivery remains a key challenge in cancer therapy, where maximizing therapeutic efficacy while minimizing side effects is critical. Although targeted drug delivery systems (DDS) have been extensively developed to achieve site-specific accumulation,[1–6] prodrug cancer therapy offers an alternative approach by relying on local chemical activation to limit systemic toxicity. In this strategy, inactive drug precursors are administered systemically and subsequently activated selectively within tumor tissues.[7–9] The selectivity of prodrug activation relies on precise spatial control at targeted tumor sites and chemical specificity toward the intended prodrug molecules.

Among emerging strategies, catalytic prodrug activation has garnered significant attention. This approach employs catalysts to selectively and efficiently convert prodrugs into their active forms at designated locations and times. Both enzymatic and metal-based catalysts have been actively investigated for this purpose. Enzymatic catalysts exhibit excellent biocompatibility and substrate specificity but are often limited to natural transformations,[10,11] requiring elaborate protein engineering for broader applications. In contrast, metal catalysts offer greater versatility owing to their tunable metal centers and coordination environments, enabling a broader range of chemical transformations, particularly in bio-orthogonal contexts.[12–18] Among various protecting groups used in prodrug strategies, the *N*-propargyl group is particularly advantageous due to its high stability under physiological conditions and selective deprotection *via* metal-mediated reactions.[15,16] This bio-orthogonal reactivity allows for precise control over drug activation using exogenous catalytic triggers without interfering with endogenous biological processes. Such properties make *N*-propargyl groups ideal for spatially and temporally controlled prodrug activation in cancer therapy. Among metal complexes explored for bio-orthogonal catalysis, several exhibit intrinsic therapeutic properties in addition to catalytic activity. Notably, platinum-based complexes, such as cisplatin, not only serve as chemotherapeutic agents but also demonstrate catalytic potential, making them attractive candidates for dual-functional prodrug activation systems.[19,20] Despite this potential, integration of catalytic and therapeutic functions has remained underexplored.[21,22] In addition to these functional challenges, small-molecule metal catalysts often suffer from rapid systemic clearance and insufficient tumor accumulation, significantly limiting their therapeutic applicability *in vivo*.

To address these challenges, conjugating metal catalysts into polymeric carriers or molecular assemblies has emerged as a promising strategy.[23,24] This approach may help reduce

Department of Chemistry and Materials Science, Shinshu University, 3-15-1, Tokida, Ueda, Nagano 386-8567, Japan. E-mail: nishimura_tomoki@shinshu-u.ac.jp

† Electronic supplementary information (ESI) available. See DOI: https://doi.org/10.1039/d5ma00518c

renal clearance, enhance *in vivo* blood retention, and promote selective accumulation in tumor tissues *via* the enhanced permeability and retention (EPR) effect. Based on this concept, we envisioned a micellar system in which a cisplatin-based metal catalyst is immobilized on polymeric assemblies. Such a system would enable the controlled release of catalytically active species under reductive conditions, allow for the *in situ* activation of anticancer prodrugs, and maintain both catalytic and therapeutic functions. Such a carrier-based approach may offer a promising route toward improved biodistribution and tumor targeting in future *in vivo* applications.

Herein, we report the development of a polymeric micellar catalytic system comprising a cisplatin-based metal catalyst immobilized on the surface of polymeric micelles composed of poly(acrylic acid)-*graft*-poly(propylene oxide) (PAA-*g*-PPO) (Fig. 1). PAA was selected as the hydrophilic backbone due to its high density of carboxylic acid groups, which allow for efficient functionalization with metal complexes and provide favorable aqueous solubility for micelle formation.[25,26] PPO was introduced as the hydrophobic graft segment due to its ability to drive self-assembly, enabling the formation of well-defined molecular assemblies.[27–30] Under physiological reducing conditions, this system effectively released active catalytic species capable of converting propargyl-protected prodrugs *in situ*. Under cell culture conditions, the released platinum species maintained their catalytic activity, resulting in efficient cancer cell death. These results demonstrate the potential of this catalytic prodrug activation platform for selective drug activation and simultaneous therapeutic efficacy.

Results and discussion

Synthesis of poly(acrylic acid)-*graft*-poly(propylene oxide)

Poly(acrylic acid)-*graft*-poly(propylene oxide) (PAA-*g*-PPO) was synthesized *via* a condensation reaction between PAA and PPO. The synthetic scheme is outlined in Scheme S1 (ESI†). Briefly, propylene oxide was polymerized in the presence of the phosphazene base P4-*t*-Bu and 6-azide-1-hexanol. After 6 hours, 80% of the propylene oxide was consumed to yield the azido-functionalized PPO [N_3-PPO; M_n = 1.4 × 10^3 g mol^{-1} (from SEC); $Đ_M$ (from SEC using PEO standards for the calibration) = 1.09; degree of polymerization (DP) = 24] (Fig. S1 and S2, ESI†). The azide group was then converted into an amine group *via* the Staudinger reaction to yield amine-functionalized PPO (Fig. S3, ESI†). The disappearance of the characteristic IR band of the azide group at 2100 cm^{-1} confirmed the quantitative conversion of the azide to an amine group (Fig. S4, ESI†). Next, poly(*tert*-butyl acylate) was synthesized *via* RAFT polymerization (Fig. S5 and S6, ESI†), followed by deprotection of the *tert*-butyl group to yield poly(acrylic acid) [PAA; M_n = 5.2 × 10^4 g mol^{-1} (from MALS); $Đ_M$ (MALS) = 1.02; degree of polymerization (DP) = 722] (Fig. S7 and S8, ESI†). Finally, graft copolymers were prepared *via* a condensation reaction between PAA and amine-functionalized PPO. The degree of substitution was found to be 11 PPO groups per 100 repeating units of PAA (Fig. S9, ESI†). The graft copolymer composition used in this study was optimized to ensure stable self-assembly into well-defined micellar structures. Preliminary tests indicated that lower PPO grafting densities resulted in poor or unstable assemblies, whereas the selected composition provided the consistent formation of short cylindrical micelles. The NMR spectra of the synthesized metal complexes and 5-fluoro-1-propargyl-uracil are also provided in Fig. S10 and S11 (ESI†). Detailed synthetic procedures and representative ^{1}H NMR spectra as well as SEC traces are provided in the ESI.†

Self-assembly of the graft copolymers in aqueous solution

Graft copolymers are known to exhibit unique self-assembly behaviors due to the architectural separation of chemically distinct side chains and backbones.[31] Based on these insights, we first investigated the self-assembly behavior of the synthesized PAA-*g*-PPO graft copolymer in aqueous solution. Because the graft copolymers contain thermoresponsive PPO, they were expected to exhibit phase-transition temperatures in aqueous solutions.[32] To investigate this behavior, the thermoresponsive properties of the copolymers in water were initially examined using pyrene fluorescence measurements, which probe the formation of hydrophobic domains (Fig. S12, ESI†). The I_1/I_3 values gradually increased as the solution temperature decreased. The transition temperature (T_m) was determined to be 9 °C from the maximum value of the first derivative of the I_1/I_3 values. At around room temperature, the polymer exhibits a relatively small I_1/I_3 value of approximately 1.3, suggesting the

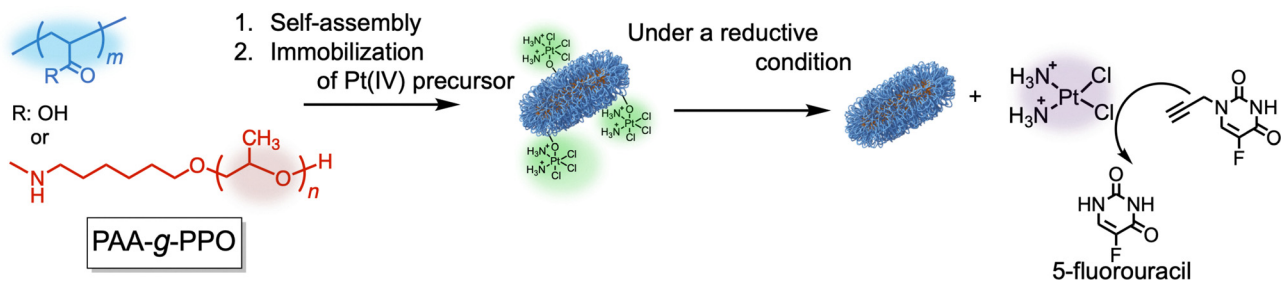

Fig. 1 Schematic illustration of self-assembly of PAA-*g*-PPO graft copolymers into cylindrical micelles and subsequent immobilization of the Pt(IV) precursor. Under a reductive condition, the Pt(IV) complex is converted to a catalytically active Pt(II) species, which deprotects propargylated 5-fluorouracil to generate the active anticancer drug.

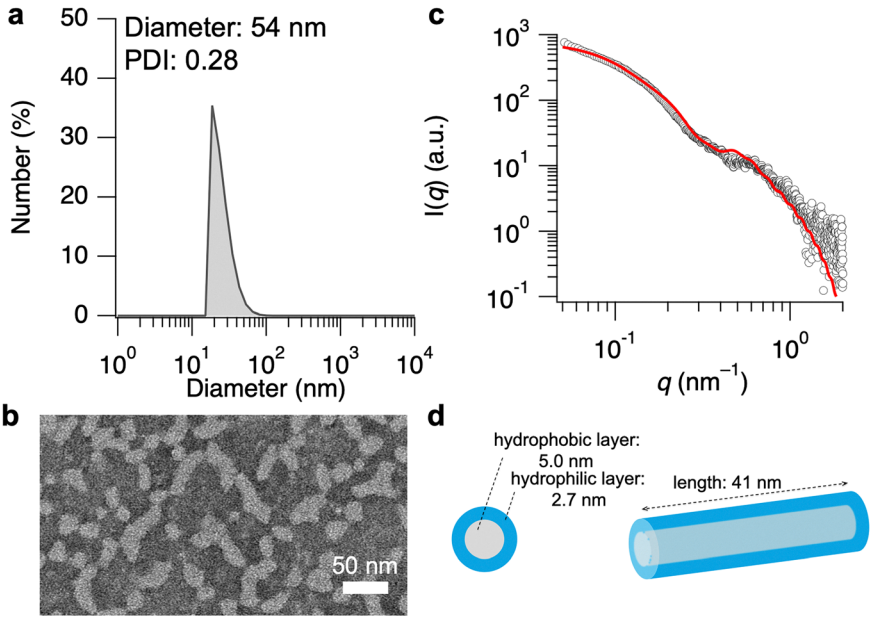

Fig. 2 (a) Size distribution of self-assembled PAA-*g*-PPO (1.0 mg mL^{-1}) in PBS. (b) TEM image of self-assembled PAA-*g*-PPO with negative staining phosphotungstic acid. (c) SAXS profile of self-assembled PAA-*g*-PPO (open circles) in PBS at 25 °C and the theoretical curve obtained using the core–shell cylinder model (red line). (d) The structural parameters of the cylindrical micelles.

formation of a hydrophobic environment and indicating that the polymer assembles in water.

We next examined the self-assembled structures of the graft copolymers in PBS buffer (pH = 7.4). To prepare the polymer solution, PBS buffer was added to a glass vial containing the graft copolymer, and the mixture was cooled to 0 °C with an ice bath to fully dissolve the polymer. The solution was then incubated at 25 °C for 1 h. Dynamic light scattering (DLS) analysis revealed an average hydrodynamic diameter of 54 nm and a polydispersity index (PDI) of 0.28 for the polymer assemblies (Fig. 2a and Fig. S13, ESI†). Transmittance electron microscopy (TEM) images of the resulting polymer solution revealed the presence of cylindrical objects with an average size of 50 nm; this value was in good agreement with the DLS (Fig. 2b).

To obtain more detailed structural information, we performed small-angle X-ray scattering (SAXS) measurements (Fig. 2c). The scattering intensities of the polymer solution in the low-q region decayed as a function of q^{-1}, suggesting the presence of cylindrical assemblies.[33] Using structural information based on the TEM observations and the characteristic feature of the SAXS profile, we attempted to fit the SAXS profile using a core–shell cylinder model.[34] The model fitted the SAXS data well over almost the entire q-range and was consistent with a radius of the hydrophobic core of 5.0 nm, a hydrophilic layer thickness of 2.7 nm, and an overall length of 41 nm (Fig. 2d and Table S1, ESI†). Overall, these data confirmed the self-assembly of the polymer into cylindrical micelles in aqueous solutions. The formation of cylindrical micelles by self-assembly of PAA-*g*-PPO is attributed to the intermediate persistence length of the PAA main chain. Based on our previous work,[28] the self-assembled nanostructure of graft copolymers is strongly influenced by the rigidity of the main chain: flexible backbones favor vesicle formation, rigid backbones promote spherical micelles, and chains with a persistence length of ~2–3 nm tend to form cylindrical micelles. Given that the reported persistence length of PAA falls within this intermediate range (1–3 nm),[35,36] the observed cylindrical morphology is consistent with these considerations.

Conjugation of platinum complexes to the polymer micelles and their release profiles

After confirming that the graft copolymers self-assembled into cylindrical micelles, we next attempted to impart catalytic functionality to the polymeric micelles. Here, we conjugated the diamine-hydroxo platinum(IV) complex onto the micellar surface.[37] The platinum complex was covalently attached to the PAA main chain using the condensation agents COMU and Oxyma (Fig. 3a). In a typical procedure, the platinum complex was added at feed ratios of 7.5, 10, and 30 equivalents per 100 acrylic acid units, with corresponding additions of COMU at 5, 10, and 20 equivalents to control the degree of modification. The reaction mixture was purified by ultrafiltration, and the degree of substitution (DS) was quantified by measuring the unreacted platinum complex in the filtrate using a colorimetric assay based on 3,4-diaminobenzoic acid (Fig. S14, ESI†).[38] As shown in Fig. 3b, DS values corresponding to 5, 9, and 25 Pt(IV) complexes per 100 acrylic acid units were achieved, indicating efficient conjugation of the platinum species into the micelles. The zeta potential of the micelles was −23 mV before Pt conjugation and increased to −12 mV after conjugation with Pt(IV) complexes at a feed ratio of 25 equivalents per 100 acrylic acid units, indicating partial neutralization of the anionic surface by the cationic Pt species. These data indicate that nearly all of the

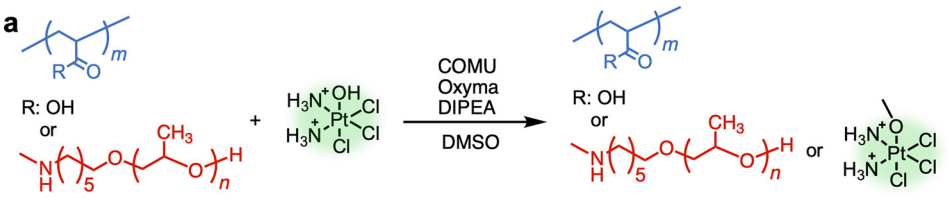

b

Equivalents of COMU per 100 acrylic acid units	Equivalents of Pt(IV) per 100 acrylic acid units	Degree of modification of Pt(IV) per 100 acrylic acid units	Diameter (nm)	PDI
0	0	0	54	0.28
5	7.5	5	44	0.24
10	10	9	46	0.24
20	30	25	40	0.25

Fig. 3 (a) Synthetic scheme for the preparation of cisplatin precursor-functionalized PAA-*g*-PPO *via* amide bond formation using COMU and Oxyma. (b) Degree of modification of Pt(IV) complexes per 100 acrylic acid units in PPO-*g*-PAA micelles at different feed ratios of the platinum precursor and COMU.

added platinum complexes were successfully conjugated onto the micelles. DLS analysis revealed that the average hydrodynamic diameter of the micelles remained approximately 40 nm after conjugation, comparable to the unmodified micelles. TEM and SAXS analyses confirmed that the micelle morphology remained cylindrical after Pt conjugation (Fig. S15, ESI†).

SAXS indicated a modest increase in electron density, consistent with the presence of Pt on the micellar surface. This observation suggests that the micellar structure and integrity were preserved following surface modification. To verify the reductive-triggered release behavior of the conjugated platinum complex, we investigated the release profile of Pt-conjugated polymeric micelles in aqueous solutions. The platinum complex used in this study has been previously reported to undergo reductive cleavage, yielding active cisplatin.[20,39,40] Pt-conjugated micelles were dispersed in phosphate-buffered saline (PBS, pH 7.4) containing sodium ascorbate at 25 °C (Fig. 4a). At predetermined time points, the dispersions were subjected to ultrafiltration, and the amount of platinum released into the filtrate was quantified by inductively coupled plasma mass spectrometry (ICP-MS). As shown in Fig. 4b, in the presence of sodium ascorbate, an initial rapid release of the platinum species was observed, followed by a sustained and gradual release over time. In contrast, in the absence of sodium ascorbate, the release was limited to the initial burst phase, with little to no further release detected thereafter. These results indicate that the reductive environment significantly promotes platinum release from the micelles.

Interestingly, the platinum release plateaued after approximately 24 hours, even under reductive conditions. One possible explanation is that positively charged or partially charged platinum species, generated during the reduction process, may undergo electrostatic adsorption onto the negatively charged micellar surfaces, thereby hindering complete release. Although further studies are required to substantiate this hypothesis, this behavior suggests complex interactions between the micellar matrix and the released platinum species. Collectively, these results demonstrate that the platinum

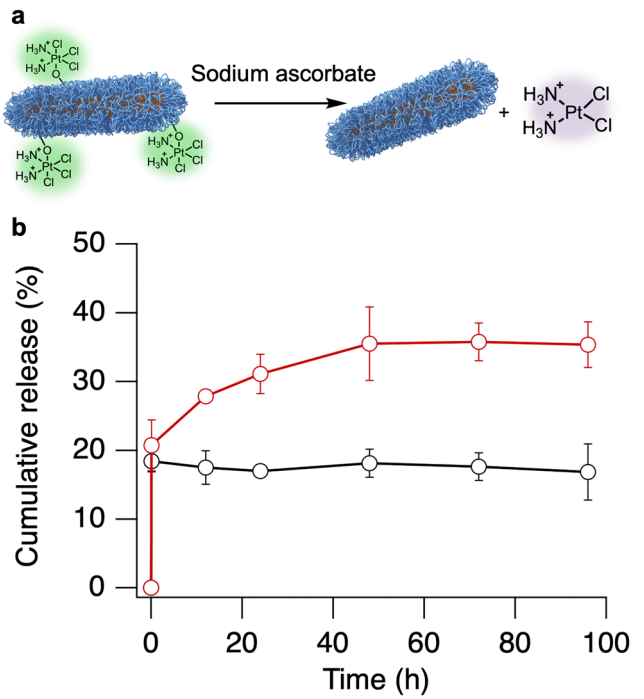

Fig. 4 (a) Schematic illustration of platinum catalyst release from cylindrical micelles in the presence of sodium ascorbate. (b) Cumulative release of the platinum catalyst from cylindrical micelles in the presence (red circles) and absence (gray circles) of sodium ascorbate at 25 °C.

complex is stably conjugated to the polymeric micelles yet can be selectively released under biologically relevant reductive conditions, supporting the design rationale for prodrug activation applications.

Activation of the 5-fluorouracil prodrug *via* reductive release of cisplatin from the polymer micelles and evaluation of cytotoxicity against cancer cells

Having confirmed that the platinum complex was successfully released from the polymer micelles in an aqueous solution, we

next turned our attention to the transformation of an anticancer prodrug into an anticancer drug by the released platinum complex. The use of metal-mediated decaging of *N*-propargyl groups has emerged as a widely studied strategy for the controlled activation of anticancer agents.[41–43] On this basis, we investigated the possibility of using *N*-propargyl groups introduced on the anticancer drug 5-fluorouracil for prodrug activation using platinum triggers. An *N*-propargyl group was used to protect a secondary amine on 5-fluorouracil to synthesize *N*-propargyl 5-fluorouracil (pFU). When pFU was treated with cisplatin in D_2O, the 6-position proton of pFU was observed at approximately 7.93 ppm in the ^{1}H NMR spectrum. As the reaction progressed, the intensity of this signal gradually decreased, and a new peak attributable to the 6-position proton of the deprotected product appeared at 7.58 ppm after 24 hours. After 36 hours, the original signal corresponding to pFU had completely disappeared, indicating that pFU was almost entirely consumed under the reaction conditions. Almost the complete consumption of pFU was confirmed by NMR measurements (Fig. S16a and c, ESI†). Consistent with this result, HPLC analysis also indicated that pFU was entirely consumed after 36 hours (Fig. S16b and c, ESI†).

To further explore the reaction conditions, we examined the influence of pH on the depropargylation process. The tumor microenvironment is known to be mildly acidic, and intracellular compartments such as endosomes also exhibit low pH, both of which may influence the reaction efficiency under physiological conditions. Incubation of pFU with cisplatin in aqueous solutions at pH 6 and pH 7 resulted in comparable initial conversion levels (Fig. S17, ESI†). After 48 hours, however, the conversion efficiency at pH 6 reached approximately 75%, whereas that at pH 7 remained at around 45%. These results indicate that the platinum-catalyzed depropargylation reaction is facilitated under mildly acidic conditions.

This enhancement is likely due to changes in the catalytic activity of cisplatin resulting from its hydrolysis and subsequent deprotonation.[44] Under physiological conditions, one of the chloride ligands in cisplatin is gradually replaced by a hydroxide ion or a water molecule through hydrolysis, generating mono-hydroxo or mono-aqua species. As the pH decreases, aquation proceeds further, and both chloride ligands can be substituted, leading to the formation of bis-aquated or mixed aquo/hydroxo species, such as $[Pt(NH_3)_2(H_2O)(OH)]^+$ and $[Pt(NH_3)_2(OH)_2]$. These species exhibit higher electrophilicity than the parent cisplatin, thereby promoting depropargylation under acidic conditions. After demonstrating that cisplatin can promote the depropargylation of pFU, we next investigated the release of the platinum complex from polymeric micelles and the subsequent depropargylation reaction mediated by the released species (Fig. 5a). To evaluate whether the released platinum complex from polymeric micelles could catalyze the depropargylation of pFU, the platinum complex-conjugated polymeric micelles were incubated with pFU in aqueous solutions at pH 6 or 7, in the presence or absence of 5 mM sodium ascorbate, and the conversion of pFU to 5-fluorouracil (FU) was analyzed by HPLC. As shown in Fig. 5b, the conversion of pFU to FU proceeded more rapidly under mildly acidic conditions

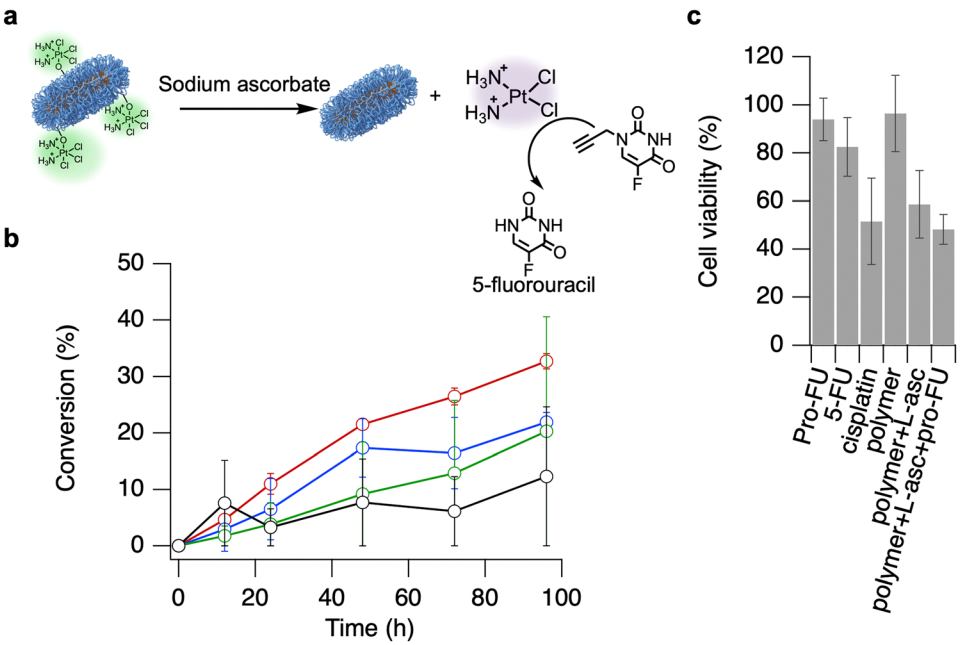

Fig. 5 (a) Schematic illustration of the release of the platinum catalyst from cylindrical micelles under reductive conditions and the subsequent depropargylation of a propargylated 5-fluorouracil prodrug to generate the active anticancer drug. (b) Time-dependent conversion of the propargylated 5-fluorouracil prodrug under four different aqueous conditions: pH = 6.0 without sodium ascorbate (green open circles), pH = 7.4 without sodium ascorbate (black open circles), pH = 6.0 with sodium ascorbate (red open circles), and pH = 7.4 with sodium ascorbate (blue open circles). (c) CT26 cell viability measured after treatment with pFU and the catalyst under specified activation conditions. Values are shown as mean ± SD (n = 6).

(pH = 6) compared to neutral conditions (pH = 7). After 96 hours, the conversion yield reached approximately 20% at pH = 6, whereas 10% conversion was observed at pH = 7. Furthermore, the presence of sodium ascorbate led to a further increase in the reaction rate, with the yield exceeding 35% under acidic conditions. These results can be attributed to the enhanced release of the platinum complex from the polymeric micelles under reductive conditions, as demonstrated in Fig. 4b, and to the pH-dependent transformation of cisplatin into more electrophilic aquated species at lower pH, which likely facilitate the depropargylation reaction.

Following the successful conversion of pFU to FU by the released platinum catalyst in aqueous solutions, we next assessed whether the same transformation could occur in a cell culture environment. Before assessing the prodrug activation, we evaluated the cytotoxicity of pFU and FU against CT26 cancer cells. As shown in Fig. S18 (ESI†), the viability of the cells treated with pFU was almost 100% at concentrations of up to 100 μM, whereas the viability of the cells treated FU decreased to *ca.* 60% upon increasing the FU concentration to 100 μM. We then performed prodrug-activation experiments using the platinum complex-conjugated polymer micelles in the presence of 100 μM of pFU. After 24 h of incubation, the cell viability was evaluated using a WST-8 assay (Fig. 5c). Neither the polymer micelles nor pFU induced a significant cytotoxic effect. When cells were treated with platinum complex-conjugated polymeric micelles in the presence of sodium ascorbate, a comparable level of cytotoxicity to that of cisplatin was observed. This result suggests that the platinum complex was successfully released from the micelles even under cell culture conditions. Furthermore, the addition of pFU to the culture medium containing platinum complex-conjugated polymeric micelles and sodium ascorbate further reduced cell viability from approximately 60% to below 50%. This finding implies that the released platinum complex catalyzed the conversion of pFU to FU. However, given the modest change in cell viability observed, future studies may focus on the activation of alternative anticancer prodrugs or the use of multiple prodrugs in combination to achieve enhanced cytotoxic effects against cancer cells.

Conclusions

In this study, we developed a polymeric micellar system based on amphiphilic poly(acrylic acid)-*graft*-poly(propylene oxide), which self-assembles into short cylindrical nanostructures with an average length of *ca.* 50 nm in aqueous solution. These micelles were successfully surface-functionalized with a cis platin-derived Pt(IV) complex *via* amide coupling, enabling the controlled release of catalytically active Pt(II) species under reductive conditions. The released platinum species catalyzed the depropargylation of an *N*-propargylated 5-fluorouracil (pFU) prodrug, achieving a maximum conversion yield of *ca.* 35% under mildly acidic conditions (pH = 6.0). Cytotoxicity assays using CT26 cells showed that the cell viability decreased from *ca.* 60% (Pt-micelle alone) to $<50\%$ when combined with pFU, indicating dual catalytic and therapeutic activity *in vitro*. These findings demonstrate that metal catalyst-functionalized polymer micelles can serve as dual-functional nanocarriers capable of mediating both therapeutic effects and catalytic transformations. While the activation efficiency and cytotoxic response observed *in vitro* were moderate, this study provides a proof-of-concept for localized prodrug activation *via* bio-orthogonal catalysis. Future work will focus on optimizing catalyst density, tuning release kinetics, and designing improved prodrug structures, as well as evaluating biodistribution and therapeutic efficacy in *in vivo* models.

Author contributions

Conceptualization and supervision: TN; synthetic work and physical measurements: KS, CI, and TN; *in vitro* experiments: KS; writing: KS and TN: All authors commented on and approved the final version of this manuscript.

Conflicts of interest

There are no conflicts to declare.

Data availability

All data supporting the findings of this study are available within the article and its ESI.†

Acknowledgements

This work was supported by the Ogasawara Memorial Foundation, the JSPS in the form of grants-in-aid for scientific research (B:22H02140, Exploratory:22K19057), the MEXT Leading Initiative for Excellent Young Researchers, the JST FOREST Program (JPMJFR201P), and the MEXT Promotion of Distinctive Joint Research Center Program (JPMXP0621467946). SAXS experiments were conducted at the BL40B2 beamline of SPring-8 under proposal numbers 2022A1095, 2022B1109, 2023A1121, 2023B1136, 2024A1067, and 2024B1105.

Notes and references

1 F. Danhier, O. Feron and V. Préat, *J. Controlled Release*, 2010, **148**, 135–146.
2 W. Poon, B. R. Kingston, B. Ouyang, W. Ngo and W. C. W. Chan, *Nat. Nanotechnol.*, 2020, **15**, 819–829.
3 V. P. Torchilin, *Nat. Rev. Drug Discovery*, 2014, **13**, 813–827.
4 H. S. El-Sawy, A. M. Al-Abd, T. A. Ahmed, K. M. El-Say and V. P. Torchilin, *ACS Nano*, 2018, **12**, 10636–10664.
5 K. Cho, X. Wang, S. Nie, Z. Chen and D. M. Shin, *Clin. Cancer Res.*, 2008, **14**, 1310–1316.
6 Y. Wang and D. S. Kohane, *Nat. Rev. Mater.*, 2017, **2**, 17020.
7 C. Ding, C. Chen, X. Zeng, H. Chen and Y. Zhao, *ACS Nano*, 2022, **16**, 13513–13553.

8 X. Zhang, X. Li, Q. You and X. Zhang, *Eur. J. Med. Chem.*, 2017, **139**, 542–563.
9 R. Bargakshatriya and S. K. Pramanik, *ChemBioChem*, 2023, **24**, e202300155.
10 R. Mooney, A. Abdul Majid, J. Batalla, A. J. Annala and K. S. Aboody, *Adv. Drug Delivery Rev.*, 2017, **118**, 35–51.
11 T. Nishimura and K. Akiyoshi, *Adv. Sci.*, 2018, **5**, 1800801.
12 Q. Fu, S. Shen, P. Sun, Z. Gu, Y. Bai, X. Wang and Z. Liu, *Chem. Soc. Rev.*, 2023, **52**, 7737–7772.
13 M. A. Miller, H. Mikula, G. Luthria, R. Li, S. Kronister, M. Prytyskach, R. H. Kohler, T. Mitchison and R. Weissleder, *ACS Nano*, 2018, **12**, 12814–12826.
14 Y. Yao, Y. Chen, C. Zhou, Q. Zhang, X. He, K. Dong, C. Yang, B. Chu and Z. Qian, *J. Mater. Chem. B*, 2024, **12**, 10818–10834.
15 A. Sousa-Castillo, A. Mariño-López, B. Puértolas and M. A. Correa-Duarte, *Angew. Chem., Int. Ed.*, 2023, **62**, e202215427.
16 E. Latocheski, G. M. Dal Forno, T. M. Ferreira, B. L. Oliveira, G. J. L. Bernardes and J. B. Domingos, *Chem. Soc. Rev.*, 2020, **49**, 7710–7729.
17 W. Wang, X. Zhang, R. Huang, C.-M. Hirschbiegel, H. Wang, Y. Ding and V. M. Rotello, *Adv. Drug Delivery Rev.*, 2021, **176**, 113893.
18 J. Li and P. R. Chen, *Nat. Chem. Biol.*, 2016, **12**, 129–137.
19 J. Wu, Y. Hu, H. Ye, S. Zhang, J. Zhu, D. Ji, Y. Zhang, Y. Ding and Z. Huang, *JACS Au*, 2022, **2**, 2339–2351.
20 T. Sun, T. Lv, J. Wu, M. Zhu, Y. Fei, J. Zhu, Y. Zhang and Z. Huang, *J. Med. Chem.*, 2020, **63**, 13899–13912.
21 X. Ling, J. Tu, J. Wang, A. Shajii, N. Kong, C. Feng, Y. Zhang, M. Yu, T. Xie, Z. Bharwani, B. M. Aljaeid, B. Shi, W. Tao and O. C. Farokhzad, *ACS Nano*, 2019, **13**, 357–370.
22 C. Chu, X. Lyu, Z. Wang, H. Jin, S. Lu, D. Xing and X. Hu, *Chem. Eng. J.*, 2020, **402**, 126125.
23 N. Graf, D. R. Bielenberg, N. Kolishetti, C. Muus, J. Banyard, O. C. Farokhzad and S. J. Lippard, *ACS Nano*, 2012, **6**, 4530–4539.
24 K. Yang, Z. Yang, G. Yu, Z. Nie, R. Wang and X. Chen, *Adv. Mater.*, 2022, **34**, 2107434.
25 M. R. Whittaker, C. N. Urbani and M. J. Monteiro, *Langmuir*, 2007, **23**, 7887–7890.
26 O. Borisova, L. Billon, M. Zaremski, B. Grassl, Z. Bakaeva, A. Lapp, P. Stepanek and O. Borisov, *Soft Matter*, 2012, **8**, 7649–7659.
27 N. Ozawa, J. H. Lee, I. Akiba and T. Nishimura, *Polym. Chem.*, 2023, **14**, 3834–3842.
28 T. Nishimura, Y. Hatatani, M. Ando, Y. Sasaki and K. Akiyoshi, *Chem. Sci.*, 2022, **13**, 5243–5251.
29 T. Nishimura, S. Fujii, K. Sakurai, Y. Sasaki and K. Akiyoshi, *Macromolecules*, 2021, **54**, 7003–7009.
30 T. Nishimura, S. Shishi, Y. Sasaki and K. Akiyoshi, *J. Am. Chem. Soc.*, 2020, **142**, 11784–11790.
31 L. I. Atanase, J. Desbrieres and G. Riess, *Prog. Polym. Sci.*, 2017, **73**, 32–60.
32 D. Roy, W. L. A. Brooks and B. S. Sumerlin, *Chem. Soc. Rev.*, 2013, **42**, 7214–7243.
33 G. V. Jensen, R. Lund, J. Gummel, T. Narayanan and J. S. Pedersen, *Angew. Chem., Int. Ed.*, 2014, **53**, 11524–11528.
34 S. Fujii, Y. Sanada, T. Nishimura, I. Akiba and K. Sakurai, *Langmuir*, 2012, **28**, 3092–3101.
35 D. G. Mintis and V. G. Mavrantzas, *J. Phys. Chem. B*, 2019, **123**, 4204–4219.
36 Y. Muroga, I. Noda and M. Nagasawa, *Macromolecules*, 1985, **18**, 1576–1579.
37 N. Kolishetti, S. Dhar, P. M. Valencia, L. Q. Lin, R. Karnik, S. J. Lippard, R. Langer and O. C. Farokhzad, *Proc. Natl. Acad. Sci. U. S. A.*, 2010, **107**, 17939–17944.
38 L. D. Johnson and G. H. Ayres, *Anal. Chem.*, 1966, **38**, 1218–1221.
39 H. Xiao, R. Qi, S. Liu, X. Hu, T. Duan, Y. Zheng, Y. Huang and X. Jing, *Biomaterials*, 2011, **32**, 7732–7739.
40 R. Qi, H. Xiao, S. Wu, Y. Li, Y. Zhang and X. Jing, *J. Mater. Chem. B*, 2015, **3**, 176–179.
41 R. M. Yusop, A. Unciti-Broceta, E. M. V. Johansson, R. M. Sánchez-Martín and M. Bradley, *Nat. Chem.*, 2011, **3**, 239–243.
42 J. T. Weiss, J. C. Dawson, K. G. Macleod, W. Rybski, C. Fraser, C. Torres-Sánchez, E. E. Patton, M. Bradley, N. O. Carragher and A. Unciti-Broceta, *Nat. Commun.*, 2014, **5**, 3277.
43 B. L. Oliveira, B. J. Stenton, V. B. Unnikrishnan, C. R. de Almeida, J. Conde, M. Negrão, F. S. S. Schneider, C. Cordeiro, M. G. Ferreira, G. F. Caramori, J. B. Domingos, R. Fior and G. J. L. Bernardes, *J. Am. Chem. Soc.*, 2020, **142**, 10869–10880.
44 J. K.-C. Lau and D. V. Deubel, *J. Chem. Theory Comput.*, 2006, **2**, 103–106.